Supplementary Information

Modulating water gas shift reaction via strong interfacial interaction between defective oxide matrix and exsolved metal nanoparticle

*Huijun Chen,[†a] Rui Huang,[†b] Myeong Gon Jang,[†b] Chaesung Lim,[b] Dongjae Shin,[b] Qiuyu Liu,[a] Heejae Yang,[b] Yan Chen,[*a] and Jeong Woo Han[*b]*

[a] School of Environment and Energy, State Key Laboratory of Pulp and Paper Engineering, South China University of Technology, Guangzhou, Guangdong 510006, China
E-mail: escheny@scut.edu.cn

[b] Department of Chemical Engineering, Pohang University of Science and Technology (POSTECH), Pohang, Gyeongbuk 37673, Republic of Korea
E-mail: jwhan@postech.ac.kr

1. Catalyst preparation for WGS

As-prepared $Pr_{0.4}Sr_{0.6}Co_{0.9-x}Fe_xNb_{0.1}O_{3-\delta}$ (x = 0.9, 0.7, 0.2) were synthesized by citrate combustion solution. Ammonium niobate (V) oxalate hydrate, praseodymium nitrate hexahydrate, strontium nitrate, cobalt nitrate hexahydrate, iron (III) nitrate nonahydrate were completely dissolved into deionized water at 80 °C. Ammonium niobate oxalate is quite unstable at high temperature, so the annealing temperature was set to be lower than 90 °C. Ethylene diamine tetraacetic acid (EDTA) was mixed to metal cations with a molar ratio of 1:2. Subsequently, citric acid was added to metal cations with a molar ratio of 1:2. The mixed solution was stirred overnight until the water was evaporated at 80 °C. The molten precursor was annealed in oven temperature at 200 °C until all the organic compounds were totally burned. The obtained fluffy and black powder was grinded in the milling ball machine at 500 rpm for 1 h. Then, it was sintered in air at 950 °C for 2 h to obtain the perovskite catalyst. Before the performance measurement and characterization, the powders were ball-milled again at 500 rpm for 4 h.

2. Catalyst characterizations

X-ray Diffraction (Rigaku, D/Max-2500-PC) with Cu Kα radiation was used to detect the crystal structures of perovskite catalyst with a scanning step of $2°\cdot min^{-1}$ in a 2θ range from 20° to 70°.

High-resolution transmission electron microscopy (HRTEM) measurement was performed on a JEM-3010 (JEOL Ltd, Japan) operated at 300 kV. A small amount of the sample was placed into a sample tube filled with a 99.9% ethanol solution. After agitating under ultrasonic environment for 30 min, one to two drops of the dispersed slurry were dipped onto a carbon-coated copper mesh (no.160) (Ted Pella Inc., CA, USA), and dried in an oven for overnight.

Quantification of oxygen vacancies experiment was performed with BELCAT II catalyst analyzer (MicrotracBEL, Corp.). For quantitative analysis, the amount of produced CO_2 was measured by exposing CO to oxygen vacancy-filled catalysts at a specific temperature. This CO_2 was produced when a lattice oxygen of the catalyst reacted with CO, leaving an oxygen vacancy; consequently, the amount of vacancies can be obtained numerically by quantifying this CO_2. 70 mg of catalyst was transferred to a quartz tube for pretreatment at 150 °C for 30 min under Ar condition (50 sccm) to eliminate impurities before the tests. The catalysts were pretreated at 350 °C for 1 hour with oxygen, before injected CO, the catalyst was purged to eliminate the physisorbed oxygen. The amount of produced CO_2 was measured by alternately exposing CO and O_2 to the catalyst at 350 °C to observe the reduction of lattice oxygen by CO. To distinguish between the reduction of active oxygen adsorbed on the surface and lattice oxygen, the process was repeated until there was no change in the amount of produced CO_2, and oxygen vacancies were quantified based on the amount of CO_2 in the last CO injection interval.

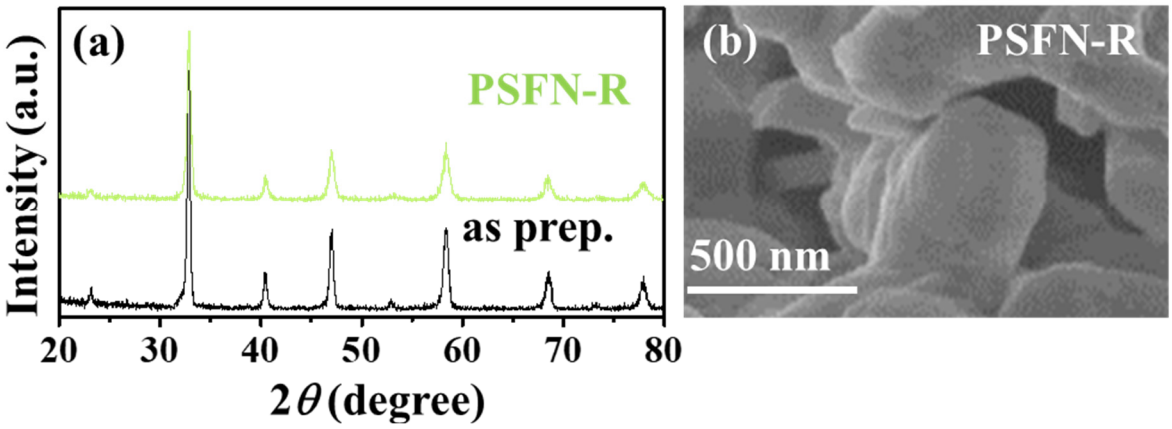

Fig. S1. (a) XRD patterns of $Pr_{0.4}Sr_{0.6}Fe_{0.9}Nb_{0.1}O_{3-\delta}$ (PSFN) in as-prepared condition and after reduction at 900 °C in 10% H_2/Ar for 2 h. (b) SEM image for reduced PSFN (PSFN-R), which shows the smooth surface without secondary phase formation.

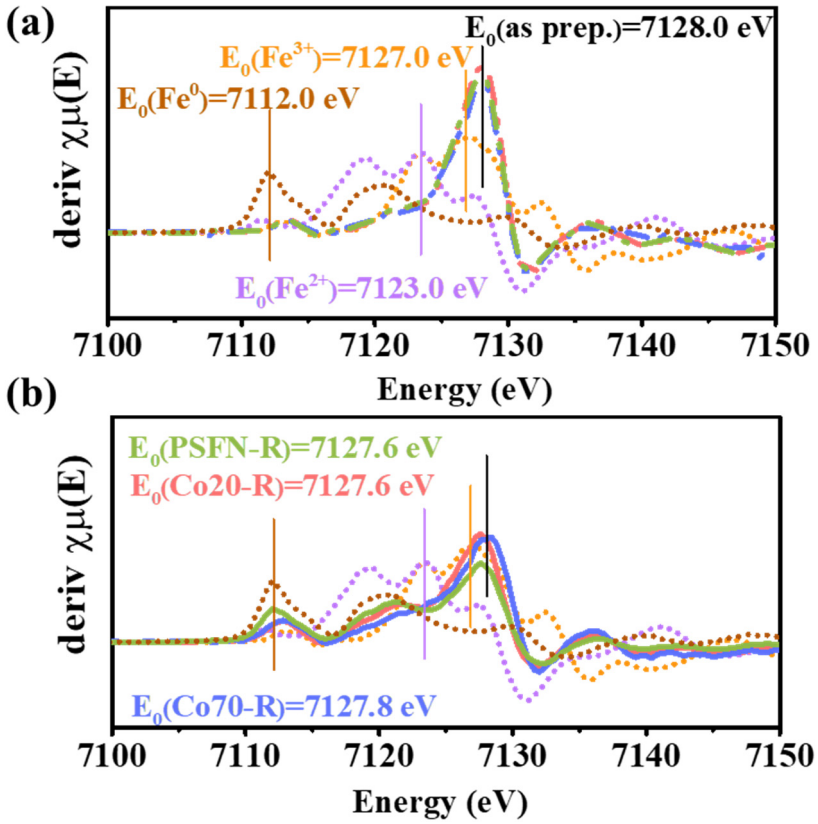

Fig. S2. First derivatives of Fe K-edge XANES spectra and the corresponding absorption edge energy (E_0) for PSCxFN (a) as-prepared and (b) reduced samples.

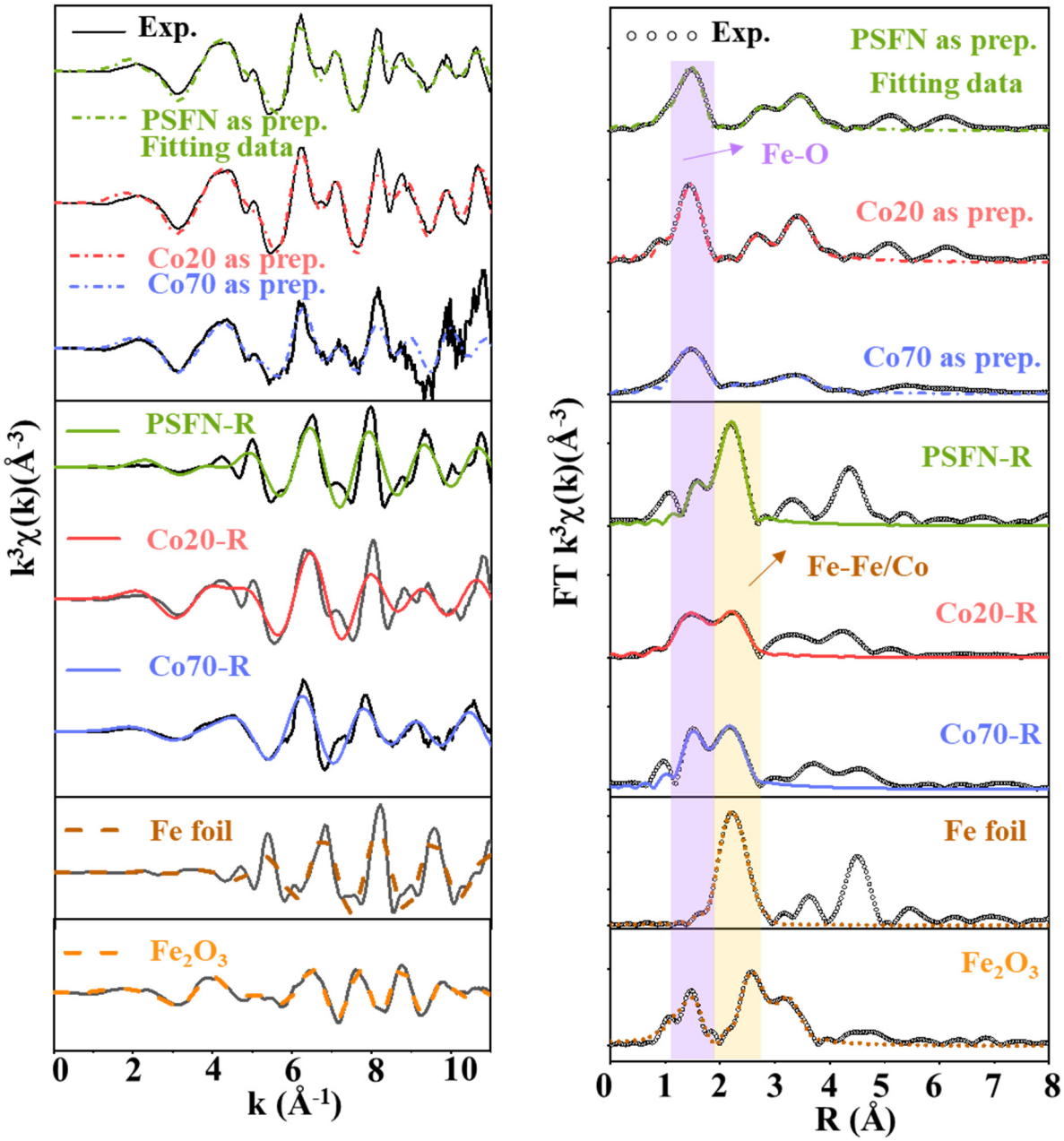

Fig. S3. Fourier-transform (FT) of Fe K-edge extended X-ray absorption fine structure (EXAFS) spectra of as-prepared and reduced PSCxFN. The weighted spectra were Fourier transformed in a *k* space of 3–11 Å^{-1}. Experimental data (Exp.) and the fitting data were shown as solid and dashed lines in the figure.

Table S1. EXAFS fitting parameters including coordination numbers (C.N.), bond distance (R), Debye-Waller factors (σ^2), inner potential correction (ΔE), and R factor for as-prepared and reduced PSCxFN powders and reference samples (S_0^2=0.75).

Sample	Path	C.N.	R (Å)	$\sigma^2\times10^3$ (Å^2)	ΔE (eV)	R factor
Fe foil	Fe-Fe	8*	2.47±0.01	5.2±0.6	6.7±1.0	0.001
	Fe-Fe	6*	2.84±0.01	6.4±1.2	5.0±2.0	
Fe_2O_3	Fe-O	6.1±1.7	1.97±0.02	12.8±3.3	-4.5±3.1	0.018
	Fe-Fe	6.7±1.2	3.00±0.01	9.2±1.4	3.2±1.9	
	Fe-Fe	3.0±.9	3.66±0.02	2.6±1.6	-9.1±3.0	
PSFN	Fe-O	6.3±0.9	1.95±0.01	-3.2±.7	-3.2±1.7	0.014
	Fe-Fe	4.2±2.4	3.20±0.04	12.2±5.3	9.4±4.6	
	Fe-Fe	4.0±.8	3.74±0.02	5.1±3.2	15.7±3.0	
Co20	Fe-O	6.1±0.6	1.94±0.01	6.0±1.0	-3.7±1.3	0.008
	Fe-Fe	3.5±1.8	3.15±0.03	9.5±4.3	6.1±4.1	
	Fe-Fe	3.4±1.2	3.71±0.02	1.9±2.2	13.7±2.4	
Co70	Fe-O	5.2±0.8	2.00±0.01	8.9±2.4	1.5±1.4	0.012
	Fe-Fe	5.0±6.1	2.98±0.08	21.7±16.2	-8.9±7.7	
	Fe-Fe	3.4±2.1	3.68±0.03	4.6±7.0	13.0±2.7	
PSFN-R	Fe-O	4.8±1.2	2.02±0.02	4.6±2.6	6.6±2.7	0.009
	Fe-Fe	4.2±0.5	2.53±0.01	5.2±0.8	4.2±1.4	
Co20-R	Fe-O	4.1±1.7	1.96±0.03	6.3±4.9	-2.7±4.2	0.010
	Fe-Fe	2.9±1.5	2.53±0.03	7.3±4.6	4.7±4.5	
Co70-R	Fe-O	3.5±1.0	2.00±0.02	3.3±2.7	-1.9±3.6	0.016
	Fe-Fe	3.2±0.8	2.54±0.02	5.2±2.0	-4.8±3.3	

*The experimental EXAFS of metal foil was fitted by fixing CN as the known crystallographic value.

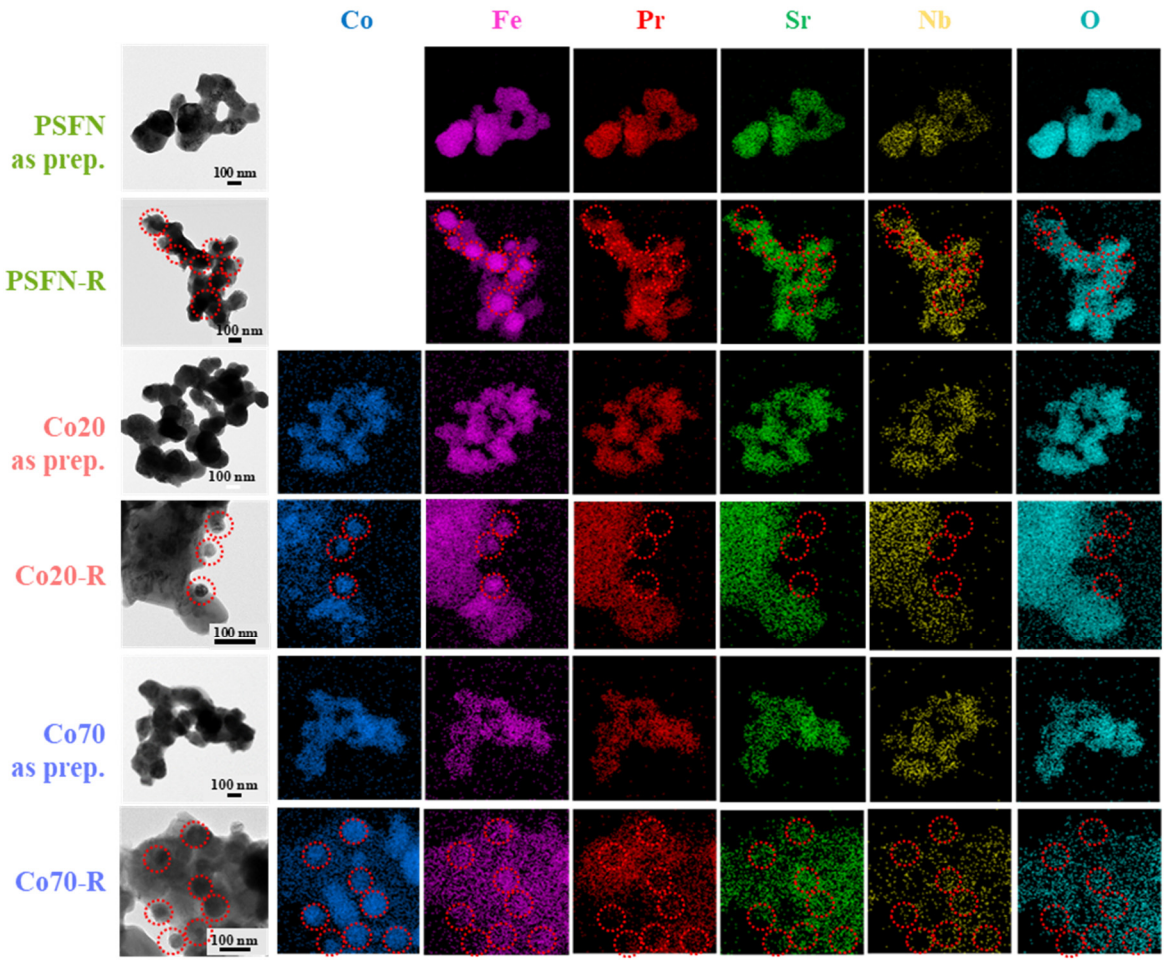

Fig. S4. HRTEM images and EDS-mapping for as-prepared and reduced PSCxFN powders. The red circles are the marks for the exsolved nanoparticles.

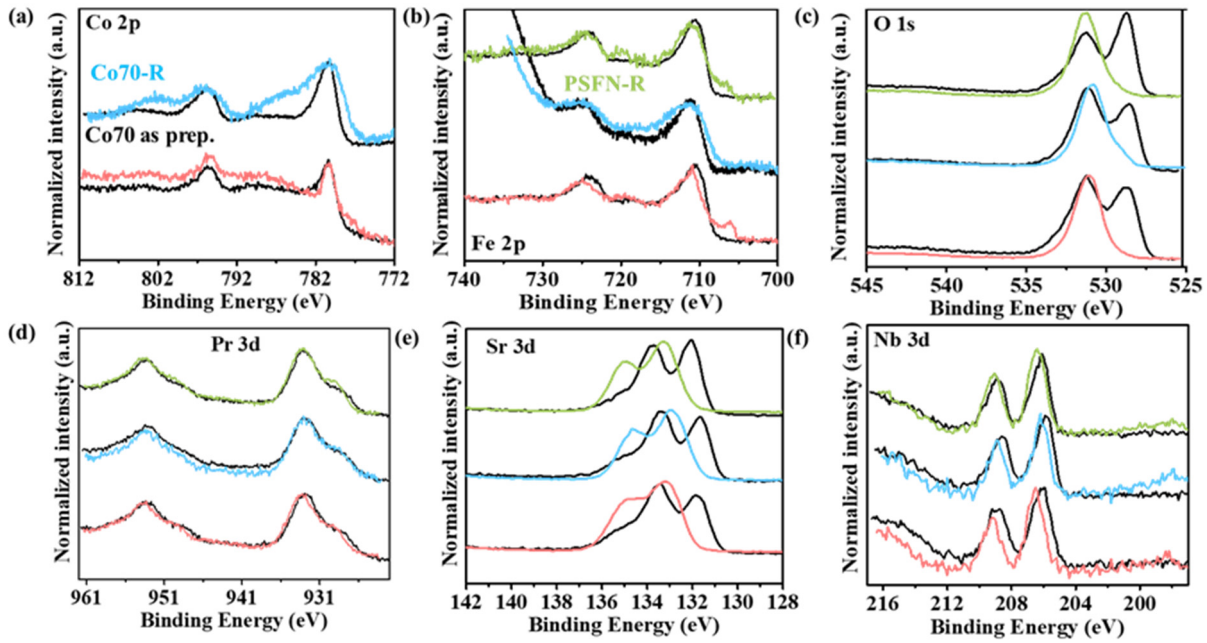

Fig. S5. XPS spectra for as-prepared (black line) and reduced PSCxFN samples (pink for Co20-R, blue for Co70-R, and green for PSFN-R).

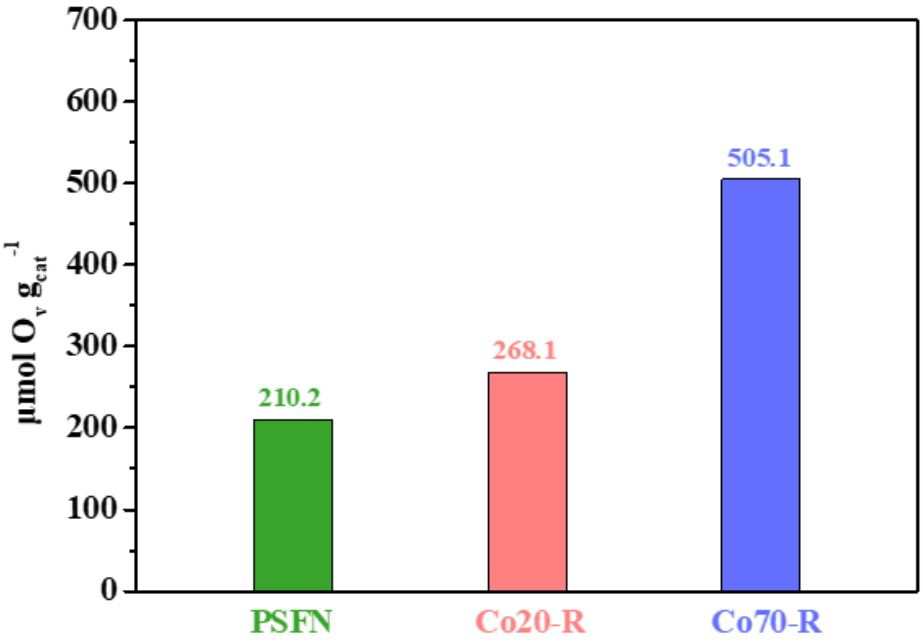

Figure S6. Quantification of oxygen vacancies in catalysts.

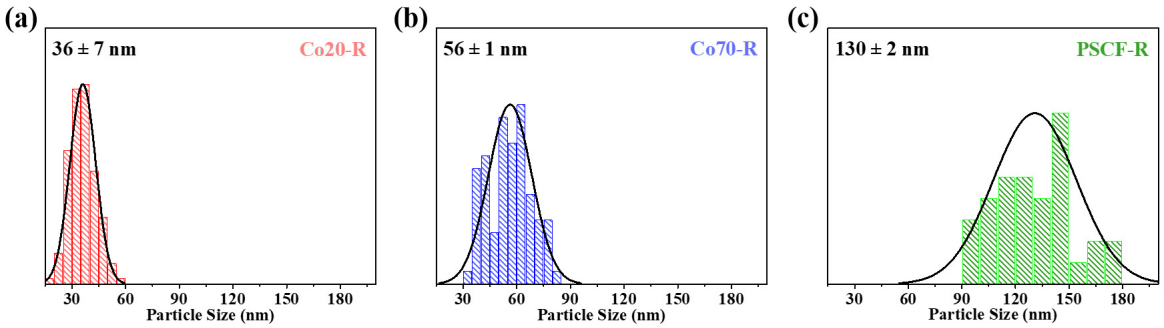

Figure S7. Size distribution of exsolved nanoparticles on the catalysts (a) Co20-R, (b) Co70-R, and (c) PSFN-R; the particle size is determined using SEM images.

3. Catalytic performance and experimental mechanistic studies

The temperature-programmed desorption (TPD) and temperature-programmed surface reaction (TPSR) measurements were performed in a quartz tube reaction system BELCAT-M (MicrotracBEL, Corp.). 30 mg of catalyst was transferred to a quartz tube for pretreatment at 1000 °C for 30 min under Ar condition to eliminate impurities before the TPD tests. To operate temperature-programmed desorption of CO (CO-TPD), the samples were pretreated at 150 °C for 30 min under He condition, and then 10% CO/He (30 mL/min) was introduced at room temperature for CO adsorption, followed by He stream (30 mL/min) purging for 30 min. Then, CO-TPD was performed in a He stream (30 mL/min) from room temperature to 1000 ℃. 70 mg of catalyst was transferred to a quartz tube for pretreatment at 150 °C for 1 h under Ar condition before the TPSR tests. In the TPSR experiment, 1.25 % CO and 12.5 % H_2O (balanced Ar, 50 mL/min) were simultaneously injected under elevated temperature conditions, and mass spectrometry detected the products.

$D_2O + H_2$ exchange reaction was performed with BELCAT II catalyst analyzer (MicrotracBEL, Corp.). 30 mg of catalyst was transferred to a quartz tube for pretreatment at 150 °C for 30 min under Ar condition (50 sccm) to eliminate impurities before the tests. 40 mL deuterium oxide (D_2O) (Sigma-Aldrich, 99.9 atom% D) was then introduced to the round bottom flask. The vaporizer temperature was set as 50 °C to provide proper vaper pressure while the carrier gas was He (30 sccm). After pretreatment, the reactor temperature stayed at 150 °C for another 60 min to stabilize the MS signal. With the 10% H_2 introducing to the system (10 sccm), the temperature increased from 150 °C to 500 °C with a 10 °C/min ramping rate and stayed at 500 °C for 60 min. The signals of each element (D_2O, H_2, HD, HDO, D_2, H_2O) were collected after the stabilization of signals at 150 °C.

In-situ DRIFTS was performed using a DRIFTS reaction cell (PIKE technologies) in a Fourier transform infrared spectrometer (FT-IR, Nicolet iS20, Thermo Scientific). The DRIFTS cell was connected with a gas flow inlet and outlet. The catalyst was mixed with KBr. The catalyst-loaded cell had pretreatment by flowing Ar at 100 °C for 1 h, then heated to target temperatures. After recording a background spectrum, 1.25 % CO and 12.5 % H_2O (balanced Ar) were simultaneously injected onto a sample at 160 °C and 170 °C for 35 min. After 35 min, only inert gas was injected under elevated temperature conditions. The DRIFT spectra were measured by accumulating 32 scans and were collected at 1-min intervals.

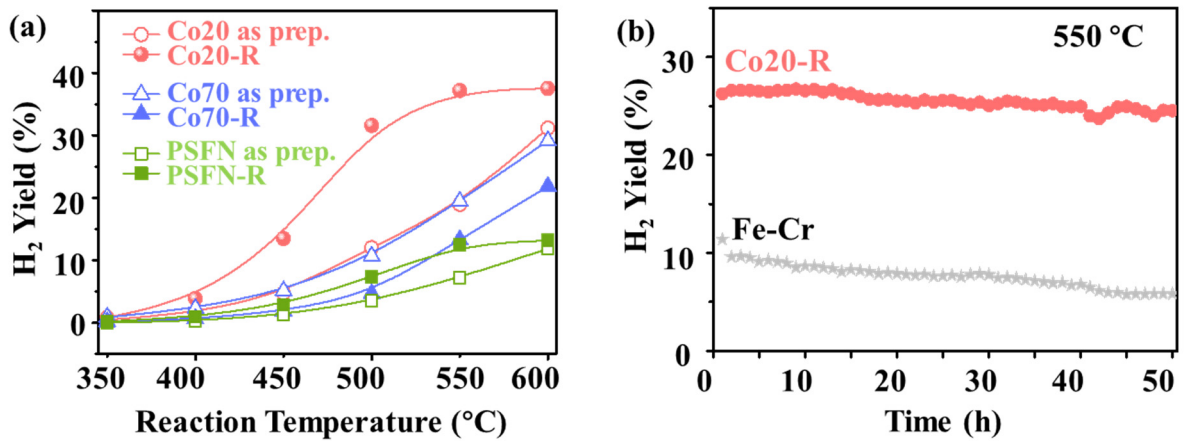

Fig. S8. Water gas shift reaction (WGS) activity and stability for PSCxFN samples with different Co contents in terms of H_2 yield. (a) H_2 yield of as-prepared and reduced PSCxFN at different temperatures. (b) Comparison of H_2 yield stability between Co20-R and commercial Fe-Cr at 550 °C.

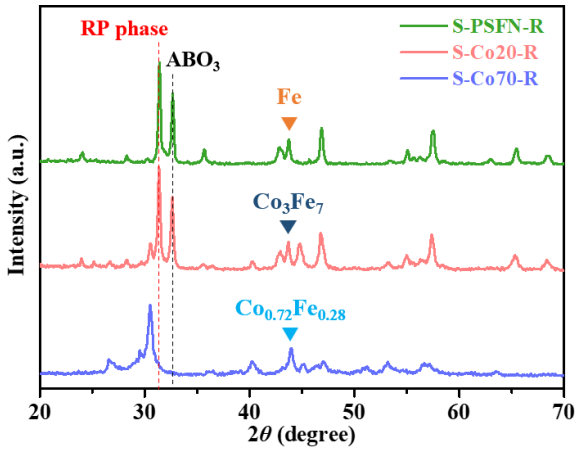

Figure S9. X-ray diffraction patterns of spent Co20-R (S-Co20-R), Co70-R (S-Co70-R), and PSFN-R (S-PSFN-R).

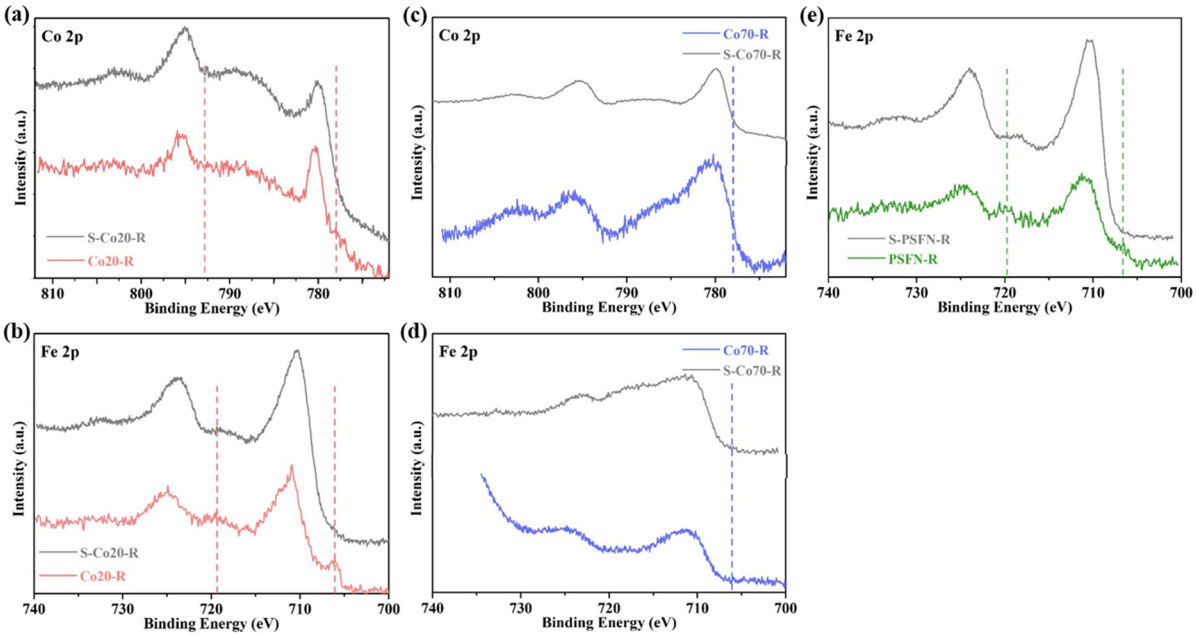

Figure S10. (a), (c) Co 2p and (b), (d), (e) Fe 2p X-ray photoelectron spectroscopy (XPS) spectra of (a), (b) Co20-R, (c), (d) Co70-R, and (e) PSFN-R; fresh catalysts (red, blue, and green line) and spent catalysts (gray lines).

Table S2. Performance comparison with other non-noble catalysts at 350 °C

	Catalyst	Composition of feed gas, H_2O/CO ratio	GHSV h^{-1}	Specific activity μmol/m^2·s	Stability (CO conv. decrease)	Reference
1	Ni@TiO_2	6%CO/24%H_2O in Ar, 4	66,000	0.19	stable up to 100h	[1]
2	Ni-Fe/CeO_2-ZrO_2	15%CO/10% CO_2/60% H_2 in N_2, steam	10,000	0.01	-	[2]
3	Fe/Co	10%CO/10%CO_2/60%H_2/ 20% N_2 and steam, 0.6	20,000	0.04	-	[3]
4	Fe/Al/Cu	17.1% CO/9.6%CO_2/ 1.0%CH_4/13.0%H_2/ 55.4%H_2O/3.9% N_2, 2.0	40,057	1.75	stable up to 20h	[4]
5	O_xFeCr	44% CO/40%H_2/ 15% CO_2/1% CH_4, steam	10,000	0.07	-	[5]
6	Co–CeO_2	17.02%CO/9.55%CO_2/ 1.03%CH_4/13.14%H_2/ 55.20%H_2O, in N_2, 3.2	143,000	0.61	50h, 14.0%	[6]
7	α-$Fe_{2-x}Cr_xO_3$	37%H_2/9%CO/4%CO_2/ 17 %N_2/ 33%H_2O, 2 bar, 3.7	60,000	0.32	24h, 5%	[7]
8	Co20-R	1.0%CO/23%H_2O in Ar, 23	146,000	0.21	50h, 2.6%	This work
9	Co70-R	1.0%CO/23%H_2O in Ar, 23	146,000	0.01	-	
10	PSFN-R	1.0%CO/23%H_2O in Ar, 23	146,000	0.03	-	
11	Fe-Cr	1.0%CO/23%H_2O in Ar, 23	146,000	0.04	50h, 15.0%	

Table S3. Distributions of the exsolved NPs and turnover frequencies for each sample.

Samples	Average exsolved NPs size	Density of exsovled NPs[1]	Turnover frequency[2]
unit	nm	ea/m^2	s^{-1}
Co20-R	36±7	1.91E+14	0.026
Co70-R	56±1	8.75E+13	0.0020
PSFN-R	130±2	3.57E+13	0.0023

1. The size and density of the exsolved NPs were measured and counted from SEM images.

2. The turnover frequency was calculated assuming the interface between exsolved NPs and support as the active sites. The interface length was calculated from the density and size of exsolved NPs.

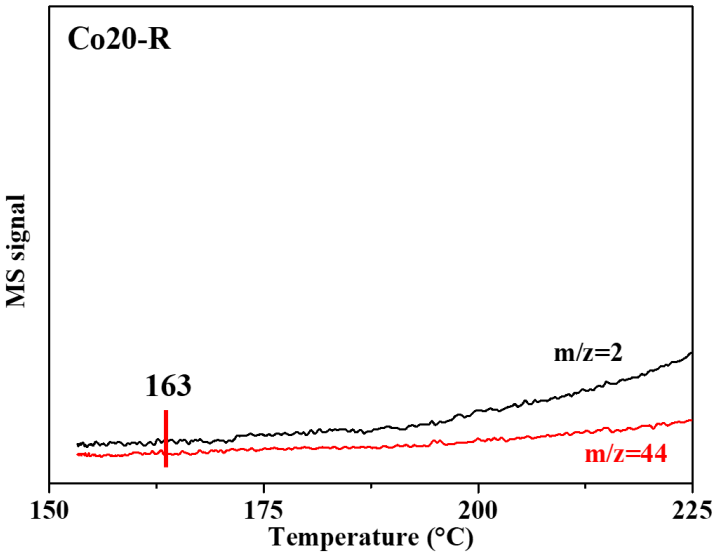

Figure S11. TPSR spectra of WGSR for Co20-R.

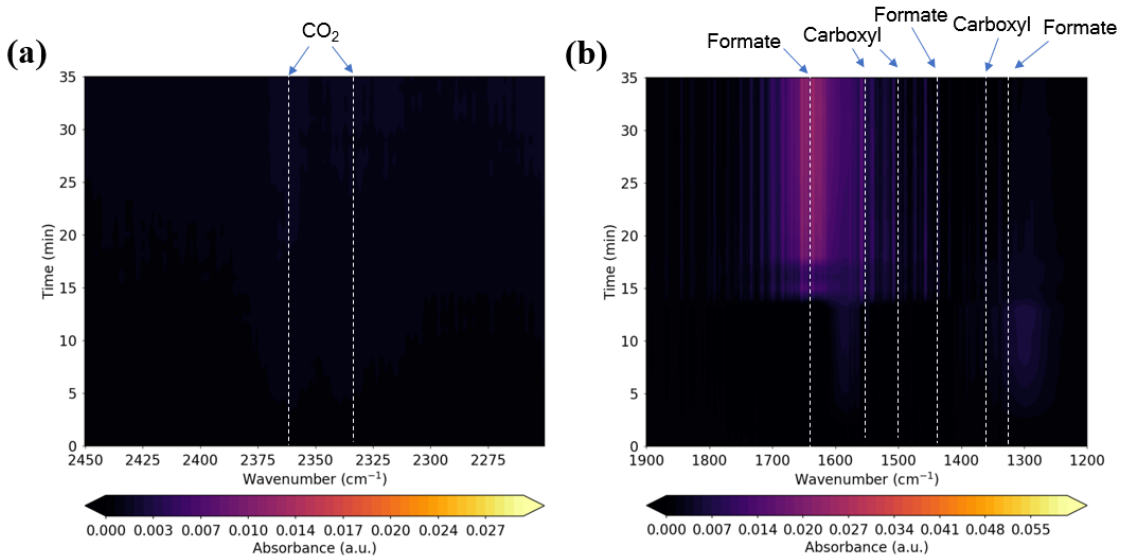

Figure S12. In-situ DRIFTS results of Co20-R at 160 °C under the WGSR for wavenumber ranges of **a** 2250 ~ 2450 cm^{-1} and **b** 1200 ~ 1900 cm^{-1}; gas injection sequence: CO + H_2O (35 min).

4. Experiment to identify the major active factor

To experimentally demonstrate that the major active factor of WGSR is oxygen vacancy, not the composition of exsolved nanoparticles, we compared the initial activities of catalysts without the influence of oxygen vacancies. The oxygen healing process was performed on the catalyst surface to minimize the effect of oxygen vacancies. This treatment may reoxidize the exsolved perovskite because it can create an oxidative condition. Therefore, the treatment was performed at a temperature above which oxygen vacancies could be filled without affecting the structure of the catalyst.[8-10] The catalysts were pretreated at 350 °C for 1 hour with oxygen, and then they were purged to eliminate the physisorbed oxygen.

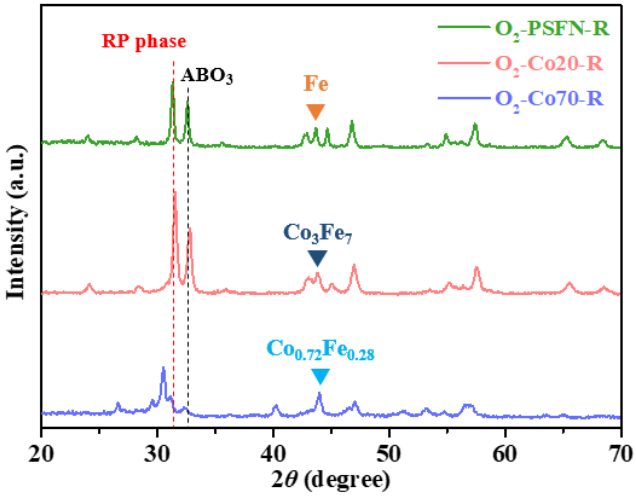

Figure S13. X-ray diffraction patterns of O_2 pretreated Co20-R (O-Co20-R), Co70-R (O-Co70-R), and PSFN-R (O-PSFN-R).

The structure of O_2-pretreated catalysts was evaluated using XRD to demonstrate that this pretreatment condition does not change the catalyst structure (Fig. S13). The exsolved nanoparticles and perovskite structure of O_2-pretreated catalysts were identical to those of fresh catalysts (Fig. 1a). Under this oxidative condition, the catalysts were neither reoxidized nor structurally changed, so we could fill the oxygen vacancies on the surface without structural changes.

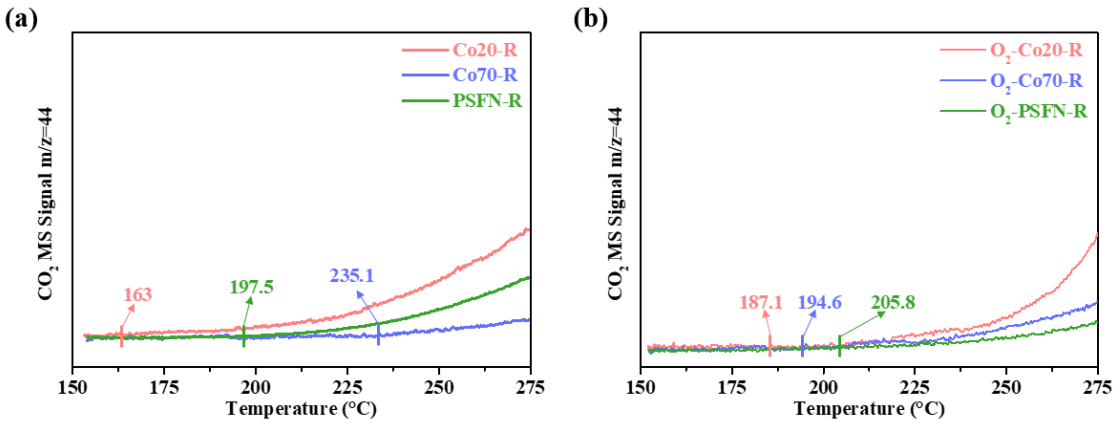

Figure S14. TPSR spectra of WGSR for (a) fresh catalysts, (b) O_2-pretreated catalysts.

Based on the oxygen vacancy healing pretreatment, the initial activation temperatures of catalysts were compared using the TPSR spectra of WGSR. When comparing the initial activities of fresh catalysts, Co20-R was activated at the lowest temperature (Fig. S14a). On the other hand, as indicated previously, Co70-R has the highest initial activation temperature due to strong CO adsorption. Therefore, the order of activation temperature was same as the reactor test reported in the manuscript (Fig. 4b).

Next, the initial activity of the O_2-pretreated catalysts was measured (Fig. S14b). The difference in the initial activation temperatures between these three catalysts becomes much smaller than that of their fresh catalysts. When the amount of oxygen vacancies was reduced by O_2-pretreatment, the reaction started at a higher temperature because oxygen vacancy significantly affected the adsorption and dissociation of H_2O.[11, 12] The initial activation temperatures of Co20-R and PSFN-R increased after O_2-pretreatment, and thus became similar to that of Co70-R which has had the highest activation temperature due to strong CO adsorption but showed increased activity after O_2-pretreatment. This is because the strong CO adsorption strength of Co70-R, which is responsible for the decreased activity, was weakened as the amount of vacancies decreased.

Nevertheless, there are slight differences in the activation temperatures of the O_2-pretreated catalysts (Fig. S14b). It is presumed that this difference in activity is mostly due to the different metal particle sizes on the oxide.[12, 13] The Co concentration can also influence the size of the exsolved nanoparticles in these three catalysts. Co20-R has the smallest particle size (36 ± 7 nm), followed by Co70-R (56 ± 1 nm) and PSFN-R (130 ± 2 nm) (Fig. S7). Therefore, the Co concentration affects the activity due to their effects on both the amount of oxygen vacancies

and the size of exsolved particle. Although the composition of exsolved nanoparticles may be affected by Co concentration, it does not have a significant effect on the activity.

4. Modeling of exsolved Fe-Co nanoparticle on PSCFN support

For the mechanism study of WGS reaction on Fe-Co nanoparticle (NP) exsolved on PSCFN support, the socketed Fe-Co nanorod model was constructed. The metal nanorod has been used for modeling of three phase boundary (TPB) consisting of metal NP, oxide support and air at the interface.[14, 15] In the exsolution model, the Fe-Co nanorod was placed in the void in which Pr, Sr, Fe, Co and O atoms had been removed to represent the anchored Fe-Co NP. (**Fig. S7a**). After the structural optimization, the exsolution model was validated to maintain well-conserved structure of nanorod, (110) facets, and the metal-support interface (**Fig. S7b, c**). The exposed (110) facet of Fe-Co NP is consistent with the TEM image of the interface structure of Fe-Co NP exsolved on PSCFN surface.[16]

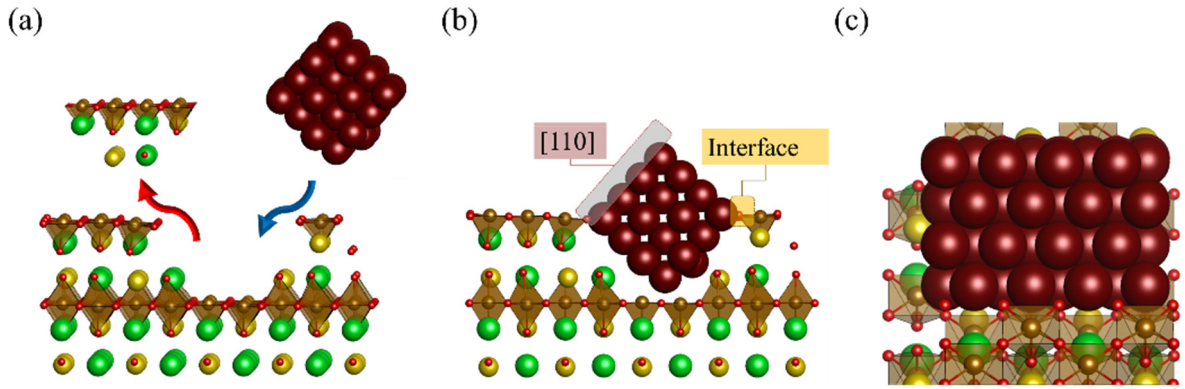

Fig. S15. Metal nanorod used for modeling of three phase boundary (TPB) consisting of metal NP, oxide support and air at the interface. (a) The void was created to make room for anchoring NP by removing Pr, Sr, Fe, Co and O atoms. (b, c) Fe-Co nanorod was placed into the void to represent the anchored Fe-Co NP.

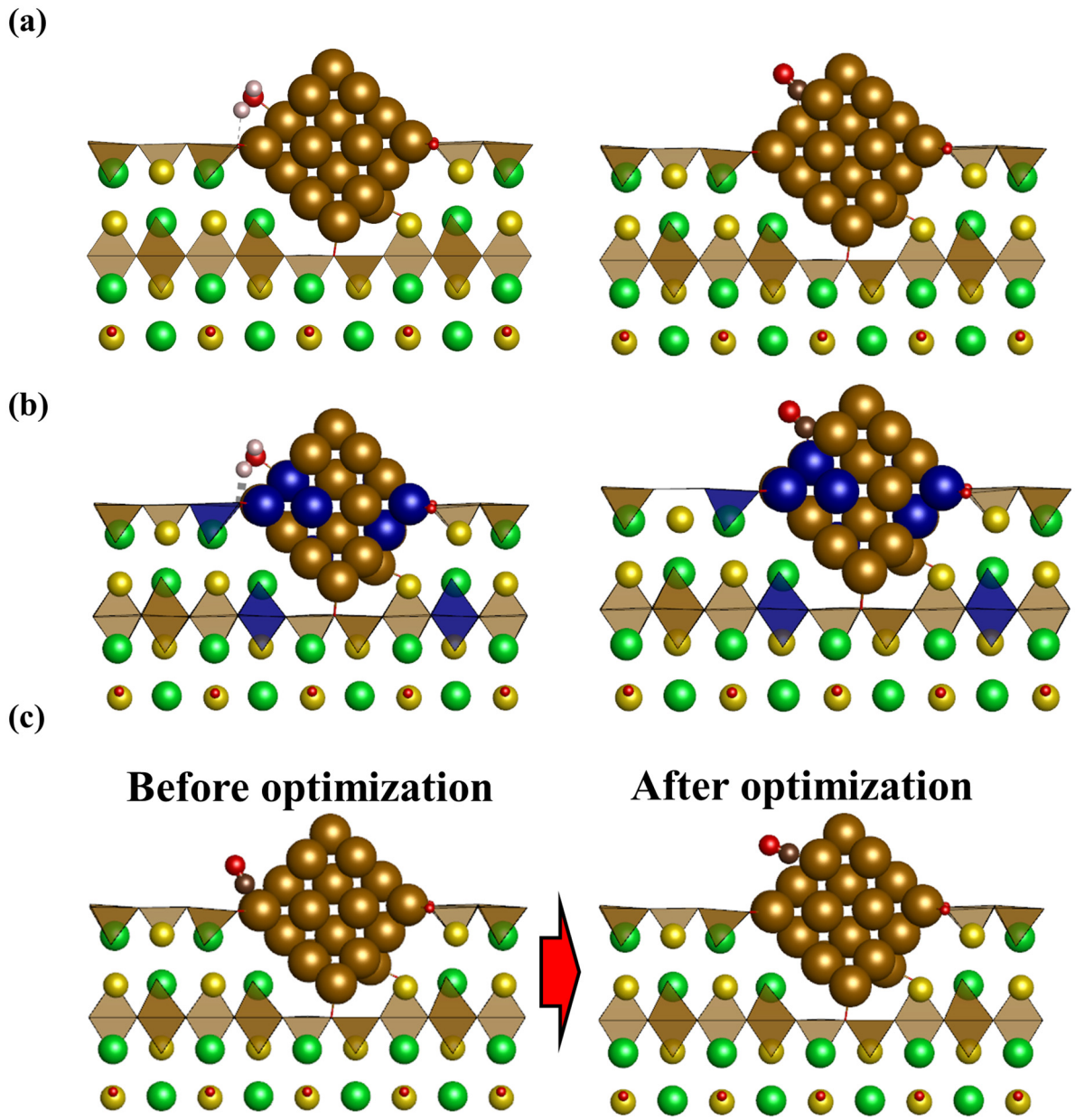

Fig. S16. (a) DFT-optimized structure of H_2O and CO adsorbed on PSFN-R. (b) DFT-optimized structure of H_2O and CO adsorbed on Co20-R. (c) Optimization process of CO adsorbed at the interfacial site of PSFN-R. After the DFT optimization, the adsorption site was changed from interfacial site to the NP site.

References

1. M. Xu, S. He, H. Chen, G. Cui, L. Zheng, B. Wang and M. Wei, *ACS Catal.*, 2017, **7**, 7600-7609.
2. K. Watanabe, T. Miyao, K. Higashiyama, H. Yamashita and M. Watanabe, *Catal. Commun.*, 2011, **12**, 976-979.
3. A. L.C. Pereira, N. A. dos Santos, M. L.O. Ferreira, A. Albornoz and M. do Carmo Rangel, in *Studies in Surface Science and Catalysis*, eds. F. Bellot Noronha, M. Schmal and E. Falabella Sousa-Aguiar, Elsevier, 2007, vol. 167, pp. 225-230.
4. D.-W. Jeong, V. Subramanian, J.-O. Shim, W.-J. Jang, Y.-C. Seo, H.-S. Roh, J. H. Gu and Y. T. Lim, *Catal. Lett.*, 2013, **143**, 438-444.
5. M. Maroño, E. Ruiz, J. M. Sánchez, C. Martos, J. Dufour and A. Ruiz, *Int. J. Hydrog. Energy*, 2009, **34**, 8921-8928.
6. A. Jha, D.-W. Jeong, Y.-L. Lee, I. W. Nah and H.-S. Roh, *RSC Adv.*, 2015, **5**, 103023-103029.
7. M. I. Ariëns, V. Chlan, P. Novák, L. G. A. van de Water, A. I. Dugulan, E. Brück and E. J. M. Hensen, *Appl. Catal. B: Environ.*, 2021, **297**, 120465.
8. R. Schaub, E. Wahlström, A. Rønnau, E. Lægsgaard, I. Stensgaard and F. Besenbacher, *Science*, 2002, **299**, 377-379.
9. Y. Chen, W. Yang, S. Gao, C. Sun and Q. Li, *ACS Appl. Nano Mater.*, 2018, **1**, 3565-3578.
10. S. B. T. Tran, H. Choi, S. Oh and J. Y. Park, *J. Catal.*, 2019, **375**, 124-134.
11. A. Chen, X. Yu, Y. Zhou, S. Miao, Y. Li, S. Kuld, J. Sehested, J. Liu, T. Aoki, S. Hong, M. F. Camellone, S. Fabris, J. Ning, C. Jin, C. Yang, A. Nefedov, C. Wöll, Y. Wang and W. Shen, *Nat. Catal.*, 2019, **2**, 334-341.
12. D. Shin, R. Huang, M. G. Jang, S. Choung, Y. Kim, K. Sung, T. Y. Kim and J. W. Han, *ACS Catal.*, 2022, **12**, 8082-8093.
13. M. Shekhar, J. Wang, W.-S. Lee, W. D. Williams, S. M. Kim, E. A. Stach, J. T. Miller, W. N. Delgass and F. H. Ribeiro, *J. Am. Chem. Soc.*, 2012, **134**, 4700-4708.
14. A. Cho, B. Hwang and J. W. Han, *Catal. Sci. Technol.,* 2020, **10**, 4544-4552.
15. M. Shishkin and T. Ziegler, *J. Phys. Chem. C*, 2009, **113**, 21667-21678.
16. H. Lv, T. Liu, X. Zhang, Y. Song, H. Matsumoto, N. Ta, C. Zeng, G. Wang and X. Bao, *Angew. Chem. Int. Ed.* 2020, **59**, 15968-15973.